Supporting Information

Gennaretti et al. 10.1073/pnas.1324220111

SI Methods

Superimposed Epoch Analysis. The Superimposed Epoch Analysis (SEA) is a statistical method that can be used to verify the presence and the significance of systematic responses in a dataset related to particular events occurring during key dates. We used SEA to test the striking agreement between the occurrence of the major volcanic eruptions of the last millennium and some cooling episodes inferred by STREC (summer temperature reconstruction for Eastern Canada). Our analysis was implemented as proposed by ref. 1, which used SEA to study connections between explosive volcanic eruptions and subsequent El Niño climate episodes. Our SEA was performed in the R environment according to the following steps:

First, two subsets of key volcanic dates from the last millennium were selected using the reconstruction of the global stratospheric volcanic sulfate aerosol injections of ref. 2. The 10 y with the highest sulfate aerosol loadings and the 10 y with loading values just below the preceding ones were considered as key dates corresponding to the 10 strongest and the 10 next strongest volcanic eruptions, respectively.

Second, the key volcanic dates were then used to generate two "eruption matrices" with the number of rows equal to the number of eruptions. In each row, we stacked the 30 STREC reconstructed values before and after each eruption date. In this way, two matrices were created with each composed of 10 rows and 61 columns. The values in the matrices were then normalized to attenuate the influence of large anomalies that could have occurred before or after a particular key volcanic date. To do so, the values in each row were divided by the maximum value of the row and, subsequently, the overall mean of the values in each matrix was subtracted from all values.

Third, dimensionless normalized composites, which represent the mean response of summer temperatures in Eastern Canada to each subset of volcanic eruptions, were obtained by averaging the values of each column for each matrix. To evaluate the significance of the obtained composites, we used a Monte Carlo randomization procedure that reshuffles blocks of two values in each row of an eruption matrix, thus creating 10,000 randomly generated eruption matrices. These matrices can then be used to generate 10,000 sets of composites and, subsequently, a random composite distribution for any specific year from a volcanic eruption (in our case, 61 distributions). We used these distributions to test the significance of the obtained composites at the 90%, 95%, and 99% confidence levels. The Monte Carlo randomization procedure is based on reshuffling blocks of two values rather than individual values because this allows randomly generated eruption matrices to be obtained with first-order autocorrelations similar to the original ones.

Fourth, to smooth out annual variations in the results of the SEA, we generated 3-y mean composites from the obtained composites and random 3-y mean composite distributions from the 10,000 randomly generated sets of composites. The final results are illustrated in Fig. 4 and show that the 10 major volcanic eruptions of the last millennium have produced highly significant cooling episodes in Eastern Canada that lasted for about two decades, while less intense volcanic eruptions had a shorter influence. For this reason, we decided also to test whether the 20 or 10 postevent summers were significantly colder than the preceding ones, for each of the 10 strongest and each of the 10 next strongest volcanic eruptions, respectively. The statistical test used was a one-tailed Wilcoxon rank–sum test (Table S2).

Bayesian Analysis of Regime Shifts. Regime shifts in the STREC time series were analyzed using a mixture of probability distributions to which a persistence structure was added. Such probabilistic models are often called hidden Markov models (HMM). Here, they provided an explicit and formal mechanism to detect shifts in the STREC time series and the length of "warm" and "cold" sequences (i.e., the regimes).

HMM are useful when it is suspected that observations in time exhibit persistence in several regimes with occasional transitions between them. While the observations come from distinct populations, it is not possible to identify exactly when the changes took place. HMM are typically specified through a hierarchical structure. In the first level, the way in which the transitions from one state to another occur is formalized. This is done by assuming that the "hidden" states follow a Markov process. The shifts and the persistence of each regime are governed by state transition probabilities. The second level represents the process that generates the data, given the current regime. For a given year, the data are generated from a statistical distribution whose parameters depend upon the current regime. In this study, two statistical probability distributions have been considered: a normal distribution and a lognormal distribution.

The parameters of the models (means, SDs, transition probabilities) are estimated using a Bayesian approach, as presented in detail in ref. 3. The estimation process involves Monte Carlo Markov Chain simulations, since no explicit algebraic solutions are available for the parameter estimates of such models. More specifically, we used Gibbs sampling.

Twelve configurations were considered to model the STREC time series. Bayesian HMM with one to six regimes and two probability distributions were applied (normal and lognormal). In this paper, we chose to compute the Schwarz information criterion (4) to select the best representation of the STREC time series between the competing models. The Schwarz criterion was calculated for each of the 12 configurations and allowed us to formally identify both the number of regimes and which probability distribution best fits the STREC time series. It is important to mention that this criterion takes into account both the statistical goodness of fit and the number of parameters that have to be estimated to achieve this particular degree of fit by imposing a penalty for increasing the number of parameters. We gave preference to the model that maximized the Schwarz criterion.

The estimation of the twelve HMM and the computation of their respective Schwarz criterion were performed in the MATLAB environment using codes developed by Évin et al. (3). The first step in Bayesian analysis is to set up a full probability model. That is, in addition to modeling the observable quantities (i.e., the STREC data) using a HMM, we must represent the prior degree of belief concerning all of the unknowns (i.e., the parameters of the model: means, SDs, and transition probabilities). Here we considered noninformative prior distributions for each parameter and let the data talk for itself. In our case, the Schwarz criterion reported evidence in favor of a four-state Bayesian HMM with normal distributions. This result, which states that a normal distribution is more suitable than a lognormal distribution for our data, is not surprising. In fact, in most meteorological and climatological studies, temperatures are assumed to be normally distributed.

In the Bayesian framework, all statistical inferences about the unknown parameters are based on the posterior distribution. Just as the prior distribution reflects beliefs about the parameters

of the HMM before experimentation, the posterior distribution reflects the updated beliefs after observing the sample data. Fig. 3*C* represents the posterior distributions of the mean temperature of each regime. These distributions do not superimpose, which indicates significant differences between the average temperatures of the four regimes. Furthermore, Fig. S4 (*Lower*) show the posterior distributions of the transition probability p_{kk} of each regime and indicate a strong persistence with a probability to stay in a given regime k greater than 0.8 for all regimes.

Finally, the posterior probabilities that each observation belongs to a given regime can be evaluated. These are presented in Fig. S4 for each regime. These graphs can be used to locate sudden changes from one regime to another and to identify historical sequences of warm or cold temperatures that may have occurred.

1. Brad Adams J, Mann ME, Ammann CM (2003) Proxy evidence for an El Niño-like response to volcanic forcing. *Nature* 426(6964):274–278.
2. Gao C, Robock A, Ammann C (2008) Volcanic forcing of climate over the past 1500 years: An improved ice core-based index for climate models. *J Geophys Res* 113(23): D23111, 10.1029/2008JD010239.
3. Évin G, Merleau J, Perreault L (2011) Two-component mixtures of normal, gamma, and Gumbel distributions for hydrological applications. *Water Resour Res* 47(8):W08525, 10.1029/2010WR010266.
4. Schwarz G (1978) Estimating the dimension of a model. *Ann Stat* 6(2):461–464.

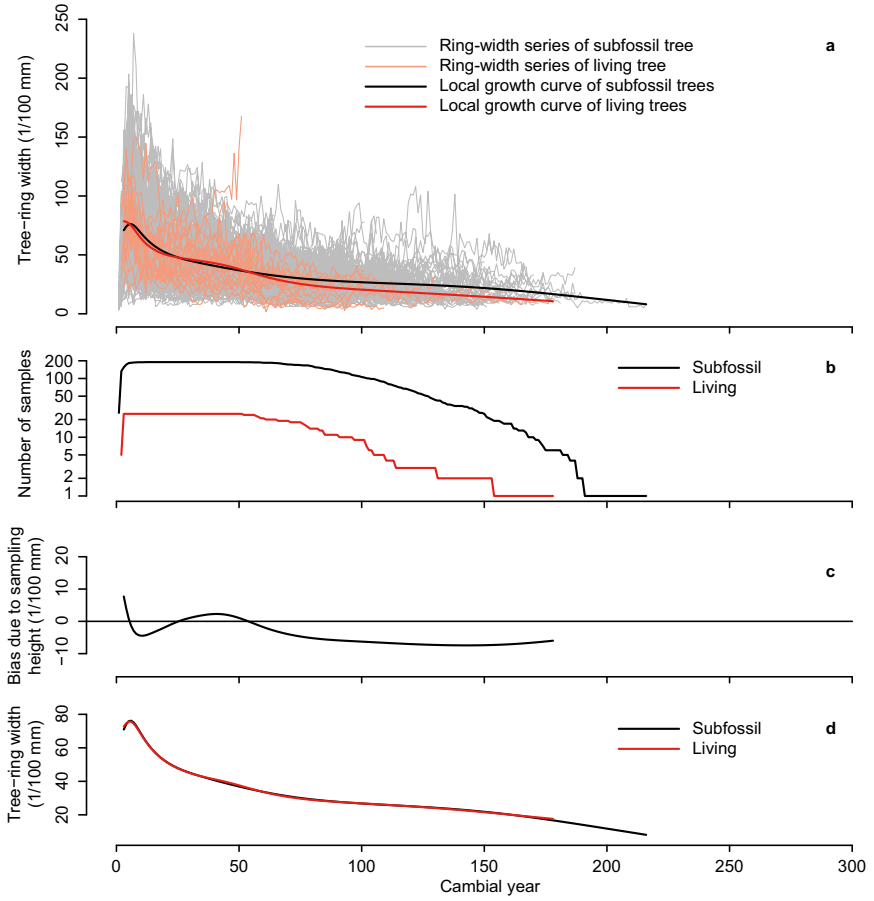

Fig. S1. Local growth curves and homogenization of subfossil and living tree materials. (*A*) The local growth curves of the subfossil and living trees at L1 (site chosen as example), (*B*) their sample replication (logarithmic *y* axis), (*C*) the bias due to sampling height (i.e., difference between local growth curves of living and subfossil trees), and (*D*) the local growth curves after the bias is removed from all ring-width series of living trees.

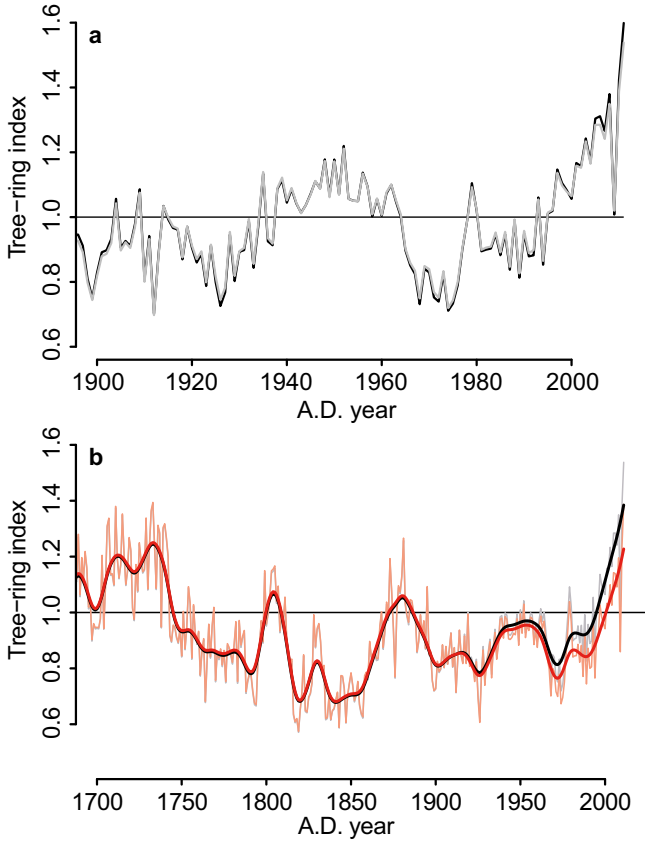

Fig. S2. Effects of removing the sampling height bias from the tree-ring series of living trees. (*A*) The Regional Curve Standardization (RCS) chronologies of L1 (site chosen as example) derived from only living trees over the last century. The local RCS chronology from uncorrected ring-width series of living trees is in black, while the same chronology from corrected series (i.e., the bias due to sampling height is removed from all ring-width series and the local growth curve of subfossil trees is used for standardization) is in gray. *A* shows that the correction of the sampling height bias is not affecting the RCS standardization results (i.e., sampling height bias can be removed and the local RCS chronology remains unchanged). The corrected ring-width series of living trees can subsequently be used together with those of subfossil samples to develop an unbiased RCS chronology (black line in *B*). The local RCS chronologies of L1 without correction of sampling height bias on the tree-ring series of living trees is shown for comparison (red line in *B*). In *B*, 20-y splines were used to smooth the values.

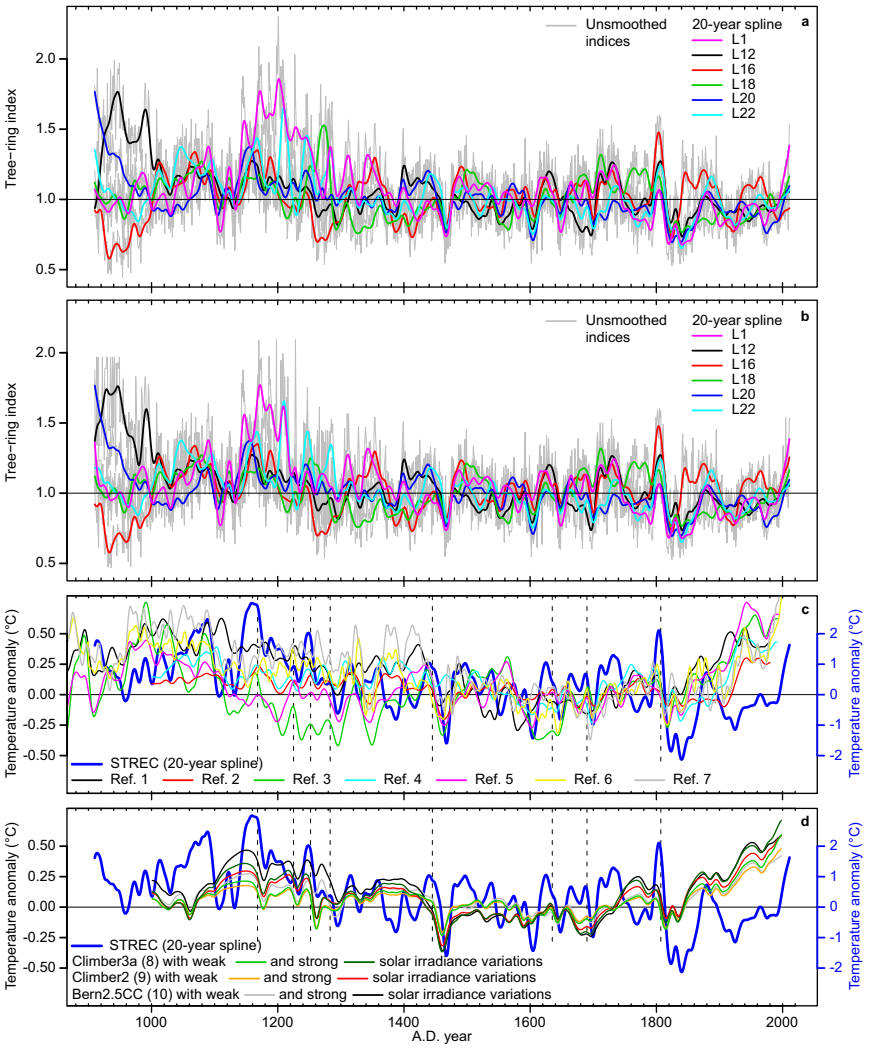

Fig. S3. The network of millennial-long tree-ring chronologies and comparison between STREC and other Northern Hemisphere records. (*A* and *B*) The six local RCS chronologies (one per lake and composed of living and subfossil trees) over the 1,102 y retained for STREC before (*A*) and after (*B*) the reconstruction of the nonrobust time intervals (i.e., intervals for each local chronology where the Rbar statistic calculated over the 31-y moving windows is lower or equal to zero or noncomputable because of low replication) using the analog method. (*C* and *D*) The comparison between STREC and seven Northern Hemisphere temperature reconstructions [refs. 1–7 (*C*)] and six Northern Hemisphere temperature simulations [three models, refs. 8–10, running twice with weak and strong solar irradiance variations and smoothed as plotted in figure 6.14 in ref. 11 (*D*)]. All records in *C* and *D* are expressed as anomalies from their 1500–1899 means. STREC has a larger variability than all other records due to its regional domain, so it is scaled on the *y* axis to improve the comparison (see blue labels). Vertical dashed lines highlight the beginning of synchronous cooling episodes in most records.

1. Moberg A, et al. (2005) Highly variable Northern Hemisphere temperatures reconstructed from low- and high-resolution proxy data. *Nature* 433(7026):613–617.
2. Mann ME, Bradley RS, Hughes MK (1999) Northern Hemisphere temperatures during the past millennium: Inferences, uncertainties, and limitations. *Geophys Res Lett* 26(6):759–762.
3. Cook ER, Esper J, D'Arrigo RD (2004) Extra-tropical Northern Hemisphere land temperature variability over the past 1000 years. *Quat Sci Rev* 23(20-22):2063–2074.
4. Jones PD, Briffa KR, Barnett TP, Tett SFB (1998) High-resolution palaeoclimatic records for the last millennium: Interpretation, integration and comparison with General Circulation Model control-run temperatures. *Holocene* 8(4):455–471.
5. D'Arrigo R, Wilson R, Jacoby G (2006) On the long-term context for late twentieth century warming. *J Geophys Res* 111(D3):D03103, 10.1029/2005JD006352.
6. Mann ME, et al. (2009) Global signatures and dynamical origins of the little ice age and medieval climate anomaly. *Science* 326(5957):1256–1260.
7. Mann ME, et al. (2008) Proxy-based reconstructions of hemispheric and global surface temperature variations over the past two millennia. *Proc Natl Acad Sci USA* 105(36): 13252–13257.
8. Montoya M, et al. (2005) The earth system model of intermediate complexity CLIMBER-3α. Part I: Description and performance for present-day conditions. *Clim Dyn* 25(2-3):237–263.
9. Petoukhov V, et al. (2000) CLIMBER-2: A climate system model of intermediate complexity. Part I: Model description and performance for present climate. *Clim Dyn* 16(1):1–17.
10. Plattner GK, Joos F, Stocker TF, Marchal O (2001) Feedback mechanisms and sensitivities of ocean carbon uptake under global warming. *Tellus B Chem Phys Meteorol* 53(5):564–592.
11. Jansen E, et al. (2007) Palaeoclimate. *Climate Change 2007: The Physical Science Basis. Contribution of Working Group I to the Fourth Assessment Report of the Intergovernmental Panel on Climate Change*, eds Solomon S, et al. (Cambridge Univ Press, Cambridge, UK), pp 433–497.

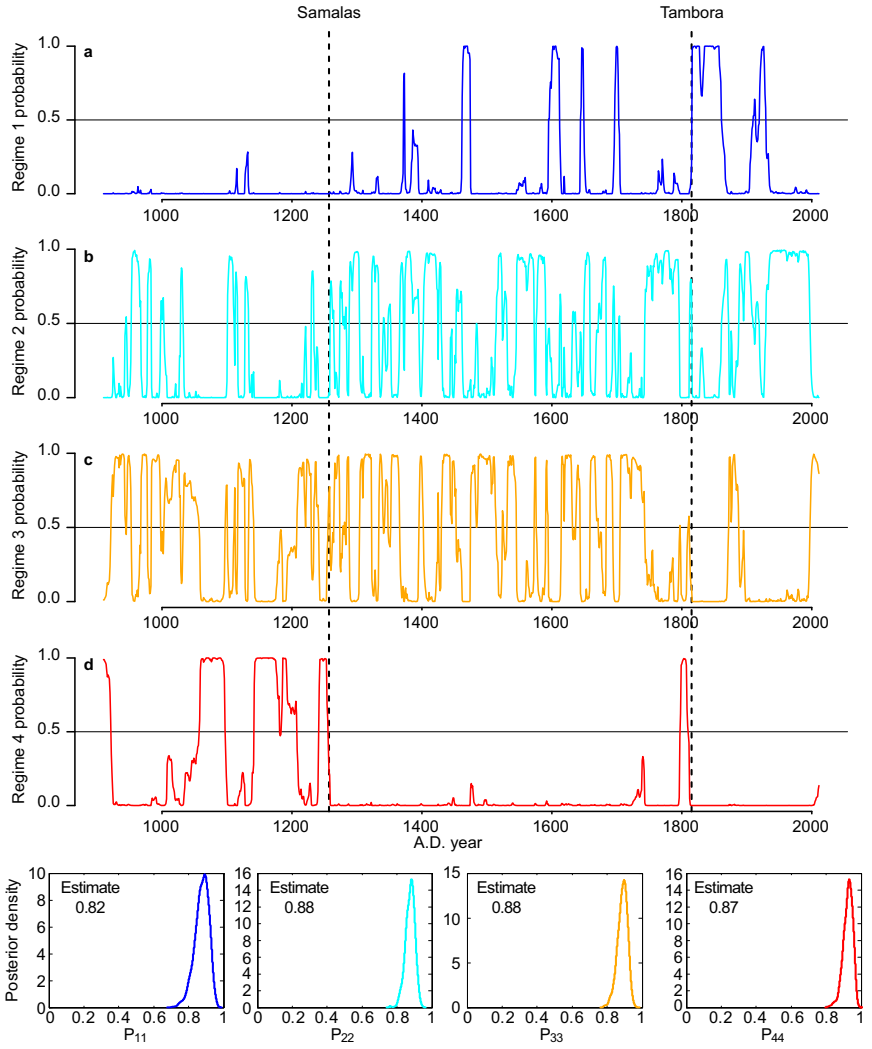

Fig. S4. Regime likelihood. Probability of STREC reconstructed temperature values to belong to any given regime of the four-component Bayesian hidden Markov model with normal distributions. (*Upper*) Regimes are ordered from the coldest to the warmest (*A*–*D*). (*Lower*) The posterior probability density functions of the transition probability p_{kk} of each regime. Regimes are ordered from the coldest (*Left*) to the warmest (*Right*).

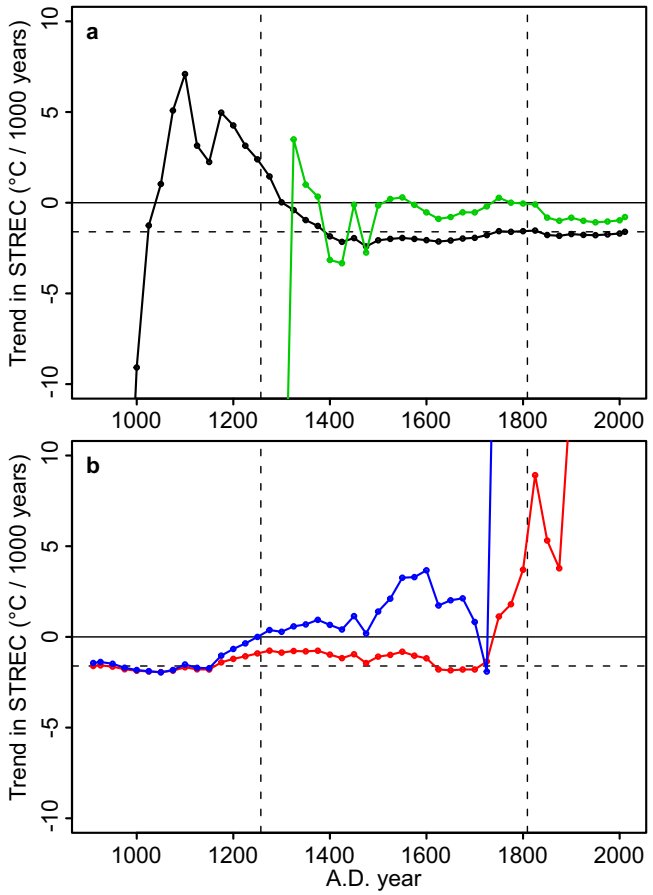

Fig. S5. Trends in STREC. In *A*, linear regression coefficients are obtained considering time periods starting from A.D. 910 (black) or A.D. 1257 (green) and increased by successive 25-y time steps (e.g., 910–950 with dot in 950, 910–975 with dot in 975...). In *B*, linear regression coefficients are obtained considering time periods starting from A.D. 2011 (red) or A.D. 1809 (blue) and lengthened backward by 25-y time steps (e.g., 1975–2011 with dot in 1975, 1950–2011 with dot in 1950...). The vertical dashed lines show the dates of the A.D. 1257 Samalas and A.D. 1809 (the event preceding the Tambora) eruptions, while the horizontal dashed line shows the trend over the entire time period covered by STREC (A.D. 910–2011; −1.6 °C per 1,000 y).

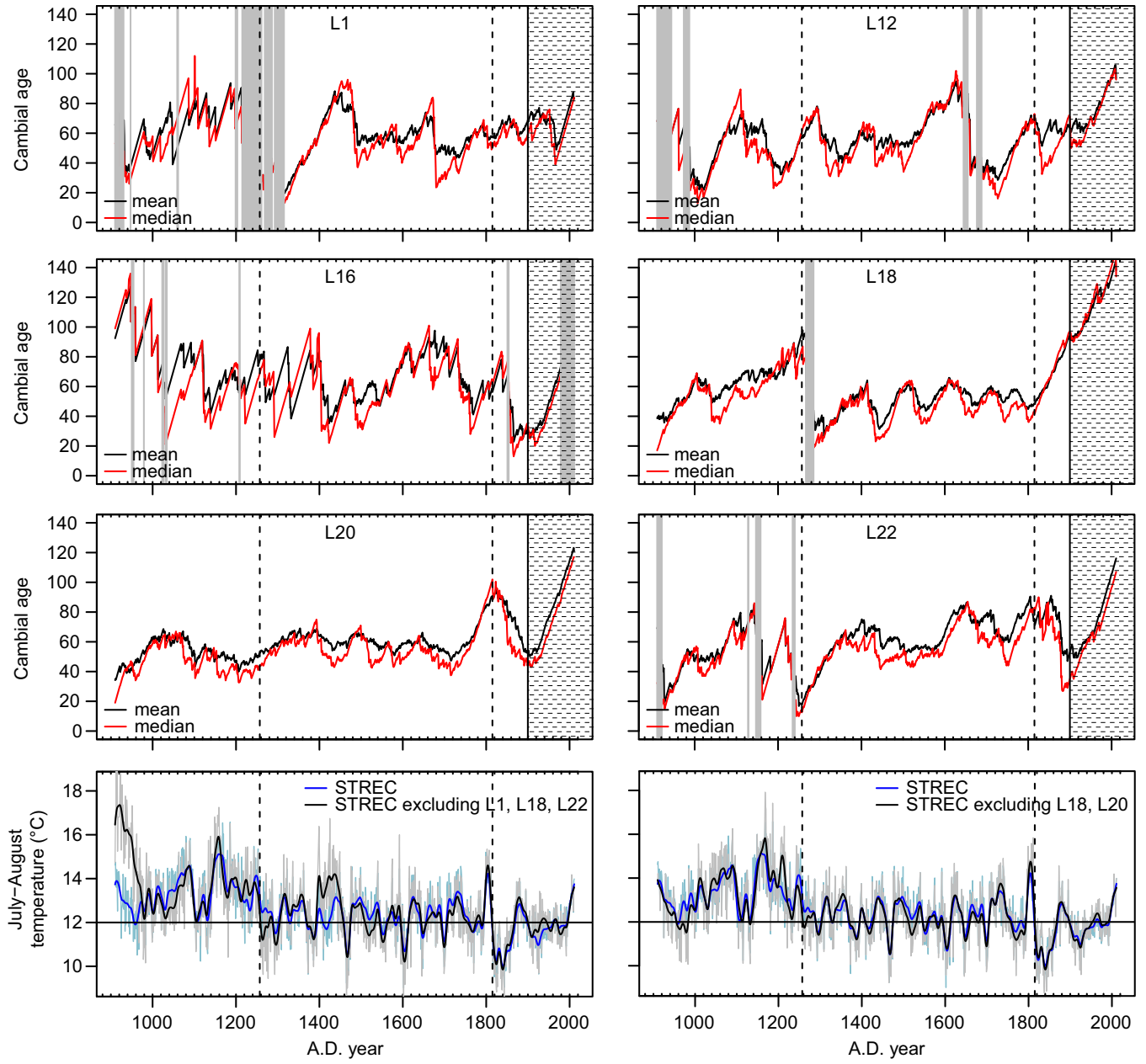

Fig. S6. (*Upper*) Time course of the mean and median cambial age for each local chronology (L1, L12, L16, L18, L20, and L22). Gray shadows show the time periods discarded for each chronology and reconstructed with the analog method. The dashed areas after A.D. 1900 show the time periods strongly influenced by living trees. The corrections applied on the ring-width series of living trees reduce possible biases in the RCS chronologies during these periods. The vertical dashed lines show the A.D. 1257 Samalas and A.D. 1815 Tambora eruptions. We tested if the most important regime shifts in STREC (i.e., post-A.D. 1257 and post-A.D. 1815) are artifacts due to local disturbances (mostly wildfires; see ref. 1) that changed the sample age structure through time in our chronologies [see *Lower* (July–August temperature)]. First, we compared STREC with an alternative reconstruction obtained by excluding those sites with unstable mean cambial age around A.D. 1257 (i.e., L1, L18, and L22). Second, we did the same exercise, but we excluded those sites with unstable mean cambial age around A.D. 1815 (i.e., L18 and L20). Smoothed values are 20-y splines. These alternative reconstructions show similar or even larger shifts at A.D. 1257 and A.D. 1815 compared with STREC suggesting that the regime shifts in STREC are robust.

1. Gennaretti F, Arseneault D, Bégin Y (2014) Millennial stocks and fluxes of large woody debris in lakes of the North American taiga. *J Ecol* 102(2):367–380.

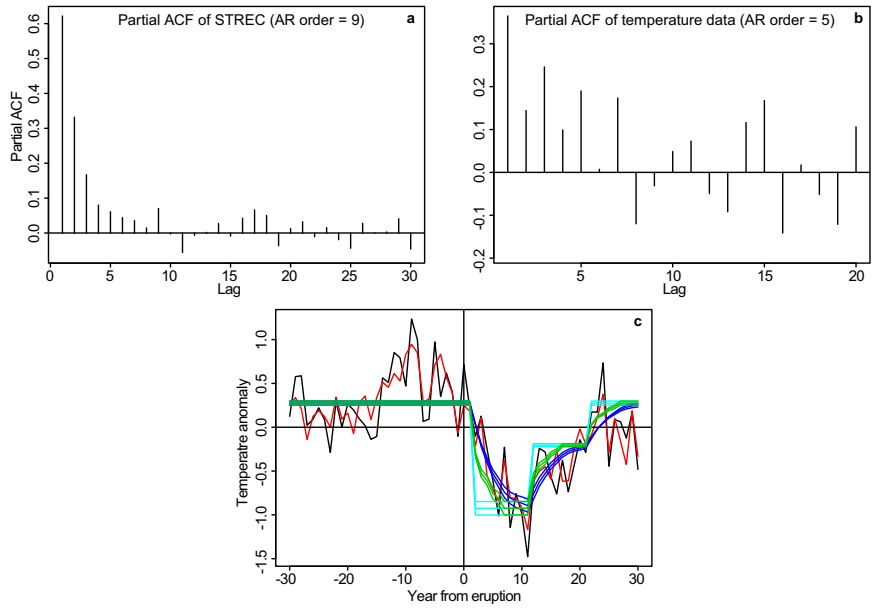

Fig. S7. Effect of autocorrelation on temperature anomalies after volcanic eruptions. (*A* and *B*) The estimates of the partial autocorrelation functions (partial ACF) fitted to STREC (*A*) and fitted to the July–August temperature data over the study area (*B*; 15 cells of the CRU TS3.20 dataset). The orders of the autoregressive model (AR order) selected by the Akaike Information Criterion are 9 and 5 for STREC and the temperature data, respectively. (*C*) The real mean (red) and median (black) responses of STREC to the 10 strongest volcanic eruptions of the last 1,100 y deduced by ref. 2, along with simulated temperature data (green) and simulated STREC (dark blue) after applying three different climate inputs (light blue) chosen to reduce the mean squared error between observed (red) and simulated (dark blue) STREC. Simulated temperature data were obtained with the formula $SimT_i = (\sum_{k=0}^{n} Input_{(i-k)} AC_k)/(\sum_{k=0}^{n} AC_k)$, where $SimT_i$ is the simulated temperature in the year *i*, *n* is the order of the autoregressive model fitted to the July–August temperature data over the study area, *k* is the lag of the partial autocorrelation function, $Input_{(i-k)}$ is the climate input in the year $(i-k)$, and AC_k is the estimate of lag *k* for the partial autocorrelation function fitted to the July–August temperature data over the study area (note that $AC_o = 1$). Here, we chose a two-step climate input composed of a constant reduction over 10 y starting from year 2 from eruptions (constant values were −1.1 °C, −1.2 °C, and −1.3 °C) followed by another constant reduction over 10 y (40% of the first reduction). Once the simulated temperatures were obtained, simulated STREC data were obtained with the formula $SimSTREC_i = (\sum_{k=0}^{n\_STREC} SimT_{(i-k)} AC\_STREC_k)/(\sum_{k=0}^{n\_STREC} AC\_STREC_k)$. The effect of autocorrelation of tree-ring data on STREC can be considered as the difference between the simulated temperatures (green) and the simulated STREC (dark blue).

Table S1. Summary of the cross-calibration verification results for the reconstruction of July–August temperatures using two different reconstruction methods

Statistics	Calibration over 1905–1957 (STREC/PLS-R)	Calibration over 1958–2011 (STREC/PLS-R)	Calibration over 1905–2011 (STREC/PLS-R)
Mean temperature of the 1905–2011 period, °C ± SD	11.9 ± 0.8/11.7 ± 0.5	11.8 ± 1.0/11.7 ± 0.8	11.9 ± 0.8/11.9 ± 0.7
Correlation over verification period	0.55/0.51	0.50/0.40	
Correlation over calibration period	0.44/0.53	0.55/0.68	
Correlation over total period	0.60/0.60	0.61/0.65	0.61/0.68
RMSE over verification period, °C	0.88/0.93	0.81/0.79	
RMSE over calibration period, °C	0.77/0.66	0.92/0.77	
RMSE over total period, °C	0.83/0.81	0.87/0.78	0.81/0.73
Significance of FDST over verification	1.00/1.00	0.76/0.99	
Significance of FDST over calibration	0.96/0.96	0.99/1.00	
Significance of FDST over total	1.00/1.00	0.98/1.00	1.00/1.00
RE	0.52/0.47	0.44/0.46	0.34/0.46*
CE	0.28/0.19	−0.07/-0.02	
RE on smoothed datasets (20-y spline)	0.85/0.73	0.90/0.70	0.83/0.90*
CE on smoothed datasets (20-y spline)	0.66/0.40	0.58/-0.17	

Reconstruction methods: a linear scaling procedure as in STREC and a reconstruction based on a partial least squares regression (PLS-R). Fifteen cells of the CRU TS3.20 dataset (1) covering our sampling sites are used as climate reference. FDST, first difference sign test (2); RE, reduction of error (3); CE, coefficient of efficiency (4).

*Computed over the total period and using the corresponding mean temperature as a reference.

1. Mitchell TD, Jones PD (2005) An improved method of constructing a database of monthly climate observations and associated high-resolution grids. *Int J Climatol* 25(6):693–712.
2. Cook ER, Kairiukstis LA (1990) *Methods of Dendrochronology: Applications in the Environmental Sciences* (Kluwer, Dordrecht, The Netherlands).
3. Fritts HC (1976) *Tree Rings and Climate* (Academic, London).
4. Briffa KR, Jones PD, Pilcher JR, Hughes MK (1988) Reconstructing summer temperatures in northern Fennoscandinavia back to AD 1700 using tree-ring data from Scots pine. *Arct Alp Res* 20(4):385–394.

Table S2. Results of the Wilcoxon rank–sum test (one-tailed)

Year of sulfate peak	Sulfate aerosol, Tg	10 or 20 y preevent mean (A), °C	10 or 20 y postevent mean (B), °C	B − A, °C	*P* value
10 strongest volcanic eruptions					
1167*	52.11	14.89	14.07	−0.83	0.02
1227*	67.52	13.06	13.18	0.12	0.54
1258*	257.91	13.70	12.43	−1.26	0.00
1275*	63.72	12.69	12.16	−0.53	0.06
1284*	54.70	12.47	11.90	−0.57	0.03
1452*	137.50	13.03	11.32	−1.71	0.00
1600*	56.59	11.97	11.44	−0.52	0.09
1783*	92.96	11.77	12.61	0.84	0.98
1809*	53.74	13.11	11.06	−2.05	0.00
1815*	109.72	13.55	10.58	−2.98	0.00
Composite*	NA	0.03†	−0.03†	−0.06†	0.00
10 next strongest volcanic eruptions					
1001‡	21.01	12.93	13.07	0.15	0.60
1176‡	45.76	14.84	13.49	−1.35	0.02
1341‡	31.14	12.46	12.46	0.00	0.43
1459‡	21.92	12.56	10.80	−1.76	0.00
1584‡	24.23	12.32	12.47	0.15	0.63
1641‡	51.59	12.47	11.37	−1.09	0.02
1693‡	27.10	12.85	11.07	−1.78	0.00
1719‡	31.48	12.99	13.08	0.09	0.76
1835‡	40.16	10.91	9.90	−1.01	0.01
1883‡	21.86	12.92	12.35	−0.57	0.02
Composite‡	NA	0.02†	−0.03†	−0.05†	0.00

The test was used to verify if the 20 or 10 postevent summers inferred by STREC were significantly colder than the preceding ones for each of the 10 strongest and each of the 10 next strongest volcanic eruptions of the last millennium (deduced by ref. 2), respectively. Composite, the average result of 10 eruptions as obtained by the SEA.

*Twenty years before and after the volcanic eruption are considered.

†Dimensionless normalized units.

‡Ten years before and after the volcanic eruption are considered.

Table S3. Extreme decades and temperature increases reconstructed by STREC

10 warmest decades			10 coldest decades			10 strongest temperature increases on a 30-y period		
Rank	Decade	Anomaly relative to 2002–2011, °C	Rank	Decade	Anomaly relative to 2002–2011, °C	Rank	Period	Increase, °C/10 y ± SE
1/90	1161–1170	1.80	1/90	1835–1844	−3.58	1/26	1128–1157	1.48 ± 0.20
2/90	1151–1160	1.68	2/90	1818–1827	−3.21	2/26	1600–1629	1.25 ± 0.21
3/90	1086–1095	1.19	3/90	1465–1474	−2.94	3/26	1462–1491	1.15 ± 0.23
4/90	1072–1081	1.00	4/90	1848–1857	−2.76	4/26	1778–1807	1.06 ± 0.20
5/90	1141–1150	0.89	5/90	1602–1611	−2.69	5/26	1852–1881	1.06 ± 0.15
6/90	1798–1807	0.87	6/90	1920–1929	−2.52	6/26	1697–1726	0.84 ± 0.20
7/90	1061–1070	0.87	7/90	1695–1704	−2.41	7/26	1293–1322	0.83 ± 0.15
8/90	1243–1252	0.83	8/90	1384–1393	−2.17	**8/26**	**1982–2011**	**0.78 ± 0.11**
9/90	1184–1193	0.73	9/90	1905–1914	−2.14	9/26	1414–1443	0.74 ± 0.15
10/90	910–919	0.61	10/90	1644–1653	−2.12	10/26	1229–1258	0.69 ± 0.20
19/90	**2002–2011**	**0.00**	**78/90**	**2002–2011**	**0.00**			

Overlapping decades or periods are excluded from the analysis. Intervals ending in 2011 are in bold.

Other Supporting Information Files

Dataset S1 (XLSX)